# The important role of electrohydrodynamics in a system of Quincke rollers

Author: Laia López Llobet
*Facultat de Física, Universitat de Barcelona, Diagonal 645, 08028 Barcelona, Spain*

Advisor: Alberto Fernández-Nieves

**Abstract:** Colloidal spheres charged superficially are expected to repel each other through electrostatic interaction. However, in systems where the spheres are confined between two charged glass surfaces, it has been seen that long-range attractive interactions can arise due to hydrodynamics, indicating that fluid flow plays a role that is important and often neglected [1]. In this project we study the role of electrohydrodynamics in a two-dimensional system of particles that are propelled by an electric field via Quincke rotation. We determine the nature and consequences of the electrohydrodynamic flows and experimentally observe that their magnitude depends on the thickness of the cell and that it increases with it. Particle clustering and alignment has also been observed and analysed.

## I. INTRODUCTION

Quincke electrorotation refers to the spontaneous rotation of synthetic particles suspended in a dielectric fluid medium in the presence of a uniform electric field, $E_0$, which must exceed a critical value, $E_c$. Due to the application of the electric field, a surface charge builds up at the particle-liquid interface because of their permittivity difference and the accumulation of charge due to ion transport between electrodes. The surface charge build up at the particle-liquid interface results in a dipolar distribution, producing a dipole oriented in a direction that is opposite to the direction of the applied electric field.

The evolution of the dipole moment is described by the charge conservation equation at the interface [2]:

$$\frac{d\vec{P}}{dt} = \frac{-1}{\tau}\left(\vec{P} + \frac{\pi\epsilon_0 a^3 \vec{E_0}}{4}\right) + \vec{\Omega} \times \left(\vec{P} - \frac{\pi\epsilon_0 a^3 \chi^\infty \vec{E_0}}{2}\right) \quad (1)$$

where $\chi^\infty \equiv \frac{\epsilon_p - \epsilon_l}{\epsilon_p + 2\epsilon_l}$, $\tau \equiv \frac{\epsilon_p + 2\epsilon_l}{2\sigma_l}$ is the Maxwell-Wagner time, $a$ is the diameter of the particle, $\epsilon_p$ and $\epsilon_l$ are the particle and liquid permittivities, respectively, $\sigma_l$ is the conductivity of the liquid and $\vec{\Omega}$ is the angular velocity of the particle.

The first term on the right-hand side of equation 1 corresponds to the spontaneous relaxation due to charge transport in solution. The second term corresponds to the advection of charges at the interface, where $\frac{\pi\epsilon_0 a^3 \chi^\infty \vec{E_0}}{2}$ corresponds to the dielectric polarization due to the permittivity discontinuity.

If the particle does not rotate the previous equation leads to $\vec{P} = -\frac{\pi\epsilon_0 a^3 \vec{E_0}}{4}$, with $\vec{P} \sim -\vec{E_0}$, as previously mentioned. In this case, we have a situation of unstable equilibrium (Fig. 1) and any small perturbation will produce an electric torque, $\vec{\Gamma}^E = \frac{\epsilon_l}{\epsilon_0}\vec{P} \times \vec{E_0}$, that will contribute to aligning $\vec{P}$ and $\vec{E_0}$, thus causing the rotation of the particle.

The dynamics of a particle undergoing Quincke rotation can be determined from equation 1 and the equation of motion:

$$I\frac{d\vec{\Omega}}{dt} = \vec{\Gamma}^E + \vec{\Gamma}^H \quad (2)$$

where I is the moment of inertia, and $\vec{\Gamma}^H = -\pi\eta a^3\vec{\Omega}$ is the viscous torque, with $\eta$ the fluid viscosity.

The expressions for $\Omega$ and $E_c$ can be obtained by solving equations 1 and 2 in steady state [2]:

$$E_c = \sqrt{\frac{2}{\pi\epsilon_l a^3(\chi^\infty + \frac{1}{2})\mu_r\tau}} \quad ; \quad \mu_r = (\pi\eta a^3)^{-1} \quad (3)$$

$$\Omega = \frac{1}{\tau}\sqrt{\left(\frac{E_0}{E_c}\right)^2 - 1} \quad (4)$$

The rotation axis is set by the random direction of the initial perturbation. In addition, the continuous rotation can be converted into a translation if the particle is near a surface; the result is the motion of the particle in an arbitrary direction perpendicular to $\vec{E_0}$ (Fig. 1).

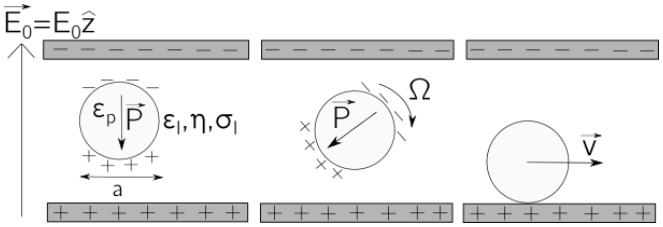


FIG. 1: Sketch of the Quincke phenomenon. The direction of the dipole is opposite to the direction of the electric field. Any perturbation results in the rotation of the particle, which leads to translation if the particle is near a wall.

Different experimental and theoretical studies have studied the dynamics, collective behaviour and density-velocity relation for systems of particles propelled by Quincke electrorotation; see, for example, [2] and [3].

However, we know from looking at the interaction between confined colloids that hydrodynamics can play a relevant role, and realize that these fluid flows have not been considered in most of the published work where Quincke rotation is exploited.

In this project, we adress the relevant interactions in a suspension of poly(methyl methacrylate) particles in a dielectric medium undergoing Quincke rotation; we do this at different packing fractions, electric field, and external conditions like relative humidity. We will see that some of our results can be understood by alluding to electrohydrodynamic flows.

## II. EXPERIMENTAL DETAILS

### A. Experimental set-up

We use poly(methyl methacrylate) spherical particles of diameter $a \simeq 60\,\mu m$ dispersed in a 0.15 mol·L$^{-1}$ docusate sodium salt (AOT)/dodecane solution, following the same concentrations as in Bricard *et al.* [2].

Initially the particles come in water solution, and therefore a transfer process is needed to disperse them in the AOT/dodecane solution. The process ensures a gradual removal from the water. The resultant dispersion is subsequently introduced as a droplet in between two ITO coated microscopy glass slides of dimensions 5 mm x 75 mm x 1 mm, with silver contact strips that act as electrodes.

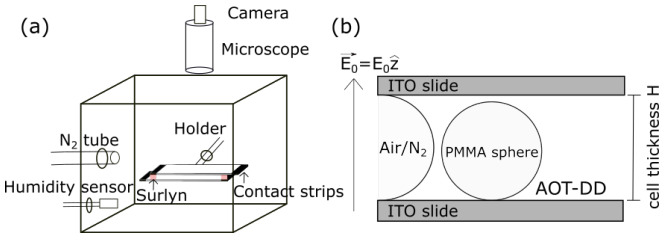


FIG. 2: (a) Experimental set-up. (b) Sketch of the side-view of the sample cell.

The experiments have been carried out in two different environments. The first one is air with relative humidity (RH) of $\sim$ 70%. The second one has a RH of $\sim$ 1-5% and is based on $N_2$. The thickness, $H$, between the two electrodes is fixed by a layer of Surlyn held by curing it at 100°C for 10 minutes. We have worked with sample thicknesses between $(65.0 \pm 0.4)\,\mu m$ and $(278 \pm 9)\,\mu m$.

The electrodes are placed under a microscope and connected to a Keysight B2987A Electrometer, used as a voltage source. The microscope is connected to a camera. We use a 0.7x magnification to visualize the system, recording images at 20 and 60 frames per second.

To measure the thickness of the sample we used an interferometer integrated with the Quincke microscopy set-up. It consists of a MWWHF2 fiber LED that couples a single warm white light emitting LED with a BFL200LS02 optical fibre, and a CCS100/M spectrometer for obtaining the spectrum, which we subsequently visualize and analize using the Thorlabs OSA software. This software allows determining the oscillations in the spectrum corresponding to Fabry Pérot's fringes, which result from the constructive interference of light between the two parallel reflecting surfaces of the glass slides. The thickness $H$ can be determined from the number of fringes p between wavelengths $\lambda_0$ and $\lambda_p$, and the refractive index of the medium $n$, which is air in our experiment [7]:

$$H = p\frac{\lambda_p \lambda_0}{2n(\lambda_0 - \lambda_p)} \tag{5}$$

### B. Tracking software

The particles have been tracked using a MATLAB script developed by D.H. Kelley and N. T. Ouellette [4], appropriately modified and adapted. The output includes the positions, instantaneous speeds and orientations of the particles in each frame as well as all the particle tracks identified. With this information, we have written a script that recognises which tracks are active in each frame and identifies clusters by interparticle distance. When two particles are sufficiently close, we take them as belonging to a cluster. We note our results do not qualitatively depend on the clustering distance threshold.

The local particle density has been calculated using Voronoi tesselation [5], which consists in dividing the space into cells obtained by drawing the intersection of the bisectors of all segments between nearby particles by means of a MATLAB routine [6]. From the local density, after multiplying by the particle area, we obtain the packing fraction $\phi$. Note this is all in two dimensions.

## III. RESULTS AND DISCUSSION

### A. AOT/dodecane-$N_2$ interface

We start by looking at the experimental setting in which we lowered the RH to $\sim$1-5% by adding $N_2$ to the humidity chamber.

In Fig. 3, we show the pair correlation function, $g(r)$, of two samples with different electric field strengths and local area fractions. From the shape of $g(r)$ we see that our system is in a liquid phase. The cohesion between the particles can be observed as a prominent peak around a center-to-center distance of $r \sim 3a$, with secondary peaks at $r \sim 6a$ and even $r \sim 9a$. At even larger $r$, $g(r) \sim 1$. In Fig. 3(b), we also observe small peaks at $r \sim 2a$ and $r \sim a$; the latter corresponds to the formation of particle duplets, which arise when the electric field is increased above $E_0 = (1.76 \pm 0.03)\,V/\mu m$.

We also observe that at sufficiently high $\phi$ and $E_0$, the particles begin to exhibit the typical Quincke phenomenon. This is, however, altered due to the attractive forces between the particles, which prevents them from exhibiting the arbitrary translation expected for Quincke rollers.

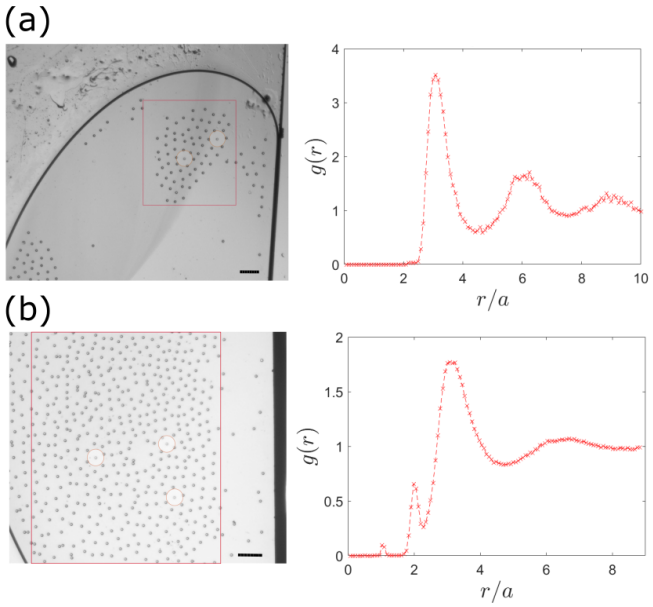


FIG. 3: (a) Pair correlation function of 993 frames of a system with $\phi = 0.094 \pm 0.003$, $H = (160 \pm 3)\ \mu m$ and electric field sweep from $E_0 = (0.94 \pm 0.02)\ V/\mu m$ to $E_0 = (1.56 \pm 0.03)\ V/\mu m$. (b) Pair correlation function of 706 frames of a system with $\phi = 0.057 \pm 0.002$, $H = (113.5 \pm 1.5)\ \mu m$ and $E_0 = (2.82 \pm 0.04)\ V/\mu m$. Scale bar 480 $\mu$m. The circles drawn have a radius R=3a.

Interestingly, we have also observed that the particles seem to adapt the average direction of motion of their neighbours. To quantify this alignment behaviour, we plot in Fig. 4 the cosine of the angle between the direction of motion of each pair of particles as a function of the distance between them.

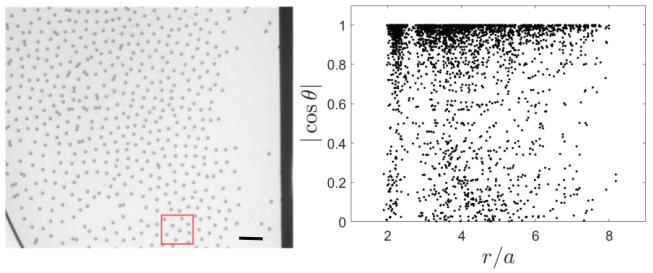


FIG. 4: Alignment analysis of 358 frames of a system with $\phi = 0.057 \pm 0.002$, $H = (113.5 \pm 1.5)\ \mu m$ and $E_0 = (2.82 \pm 0.04)\ V/\mu m$. Scale bar 480 $\mu$m.

We observe a clear alignment, corresponding to $|\cos\theta| \sim 1$, which can either be due to dipolar electric interactions or due to the hydrodynamic currents that arise as a consequence of the motion of particles in solution. Since the Debye screening length of our particles is $\sim 13$ nm, which is less than $10^{-3}a$, we attribute this alignment to hydrodynamics. We also believe that these hydrodynamic effects are responsible for the cohesion observed in the $g(r)$ data.

### B. Clustering

At high $E_0$, we observe cluster formation depending on $H$. In particular, clustering occurs for $H > (1.89 \pm 0.07)a$. No experiments were performed for thicknesses between $(1.03 \pm 0.03)a$ and $(1.89 \pm 0.07)a$; thus it is possible that the critical value for clustering is within this interval.

Fig. 5 shows an example of the clustering encountered. In Fig. 5(a), we observe the duplets seen in $g(r)$ as a peak at $r \sim a$, which spin at high velocities. The amount of duplets increases with $E_0$. In Fig. 5(b), we observe particle chains near the AOT/dodecane-$N_2$ interface during a voltage sweep.

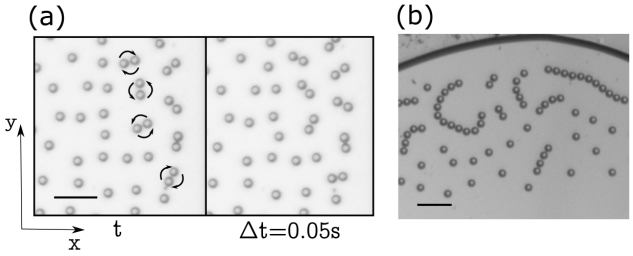


FIG. 5: Snapshot of the dynamic clusters that appear in the system. (a) $H = (113.5 \pm 1.5)\ \mu m$. $E_0 = (2.38 \pm 0.04)\ V/\mu m$. (b) $H = (160 \pm 3)\ \mu m$. The snapshot corresponds to $E_0 = (1.16 \pm 0.03) V/\mu m$ and is part of a sweep from $E_0 = (0.313 \pm 0.006)\ V/\mu m$ to $E_0 = (1.25 \pm 0.03)\ V/\mu m$. Scale bar 250 $\mu m$.

Both these phenomena as well as the small peaks of $g(r)$ at $r < 3a$ could be explained by the short-range in-plane dipole-dipole attraction of the dipole component perpendicular to $\vec{E}_0$ (Fig. 1) or due to the dipole-dipole attraction if the dipoles are aligning out-of-plane; this last regime was found by G. E. Pradillo et al (2019) [8] when the spheres do not remain at the bottom electrode. We indeed have proof that this is possible: in our experiments, at $H = (278 \pm 9)\ \mu m$, we observe that particles occasionally stack vertically thus aligning their dipoles with the electric field.

Fig. 6 shows the result of the clustering analysis in the bulk of a system with $H = (278 \pm 9)\ \mu m$ for three different electric field strengths: $E_0 = (0.90 \pm 0.03)\ V/\mu m$, $E_0 = (1.08 \pm 0.04)\ V/\mu m$ and $E_0 = (1.26 \pm 0.05)\ V/\mu m$. We obtain similar results for all $E_0$ regarding cluster abundance and cluster duration. The abundance or frequency is defined as the average number of clusters in 2000 frames. The duration corresponds to the number of frames before particles in a given cluster stray away.

We notice from Fig. 6(c) that the smallest clusters are the most frequent and the most persistent ones, with larger-particle clusters being next in abundance and duration. In Fig. 6(b), we observe that an increase in $E_0$ raises the average number of clusters we identify in a given frame.

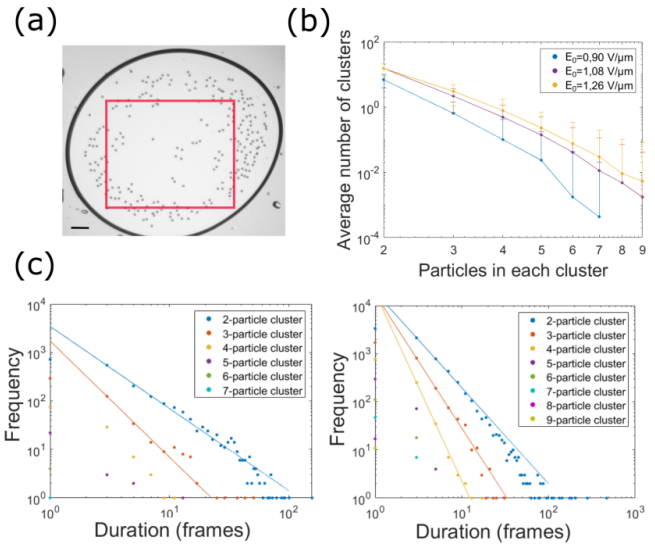


FIG. 6: Cluster behaviour at constant thickness $H = (278 \pm 9)\mu m$. (a) Area analysed. Scale bar 480 $\mu m$. (b) Dependence between the average number of clusters in one frame and the particles in each cluster for three different electric fields. Both axes are in logarithmic scale. The graph does not present negative error bars because they reach the value 0 that cannot be represented in logarithmic axes. (c) Dependence between the frequency of clusters and their duration. Each graph shows the data of 2000 consecutive frames. Left graph corresponds to $E_0 = (0.90 \pm 0.03)\ V/\mu m$. The fit equations are $\log y = (-1.69 \pm 0.07) \log x + (8.15 \pm 0.09)$ for 2-particle clusters and $\log y = (-2.39 \pm 0.18) \log x + (7.5 \pm 0.3)$ for 3-particle clusters. Right graph corresponds to $E_0 = (1.26 \pm 0.05)\ V/\mu m$. The fit equations are $\log y = (-1.99 \pm 0.02) \log x + (9.86 \pm 0.02)$ for 2-particle clusters, $\log y = (-2.79 \pm 0.08) \log x + (9.76 \pm 0.09)$ for 3-particle clusters and $\log y = (-3.9 \pm 0.4) \log x + (9.82 \pm 0.19)$ for 4-particle clusters.

### C. Electrohydrodynamic flows

Our key conjecture so far is that the long-range attractions observed in the system are due to hydrodynamics. More precisely, we believe they arise from the electrohydrodynamic flows [10] that form as a consequence of the movement of ions in solution when reaching the surface of the particles but that are unable to go through them. Once the particles are charged superficially, a flow arises when the electric field acts on the surface charge that has induced (Fig. 7).

The shape of the particles and its surface charge and electric field lines near the interface determine the shape and direction of the flows since they are a consequence of ion motion. These flows will cause effective attractions between the particles due to their rotation direction.

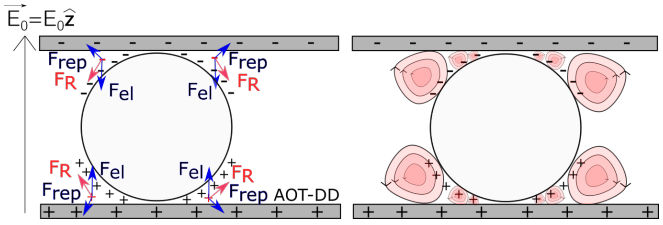


FIG. 7: Sketch of the formation of the electrohydrodynamic flows in the particle-liquid interface. $F_{rep}$ represents the repulsive force the ion experiences due to the particle surface charge, $F_{el}$ the force due to the electric field and $F_R$ the resultant force.

If the assumption that long-range attractions between particles are caused by the electrohydrodynamic flows is correct, we can then hypothesize that they will also be present near the AOT/dodecane-$N_2$ interface causing also an effective attraction of the particles to the sample boundaries. When sufficiently close, the particles will then experience a repulsive force due to the presence of like-sign charges at the AOT/dodecane-$N_2$ interface and their associated flows. We indeed observe this in our experiments [see, for example Fig. 3(a) and 5(b)]. Furthermore, we expect this repulsion to depend on $H$.

Fig. 8 shows a schematic for the formation of these electrohydrodynamic flows near the AOT/dodecane-$N_2$ interface. The $H$ dependence results from the increased effective size of ionic flows due to the accumulation of charges. Therefore, if our hypothesis is correct and since we are working with $H$ between $(65.0 \pm 0.4)\mu m$ and $(278 \pm 9)\mu m$, we should observe that the effective repulsion these flows induce should increase with increasing $H/a$.

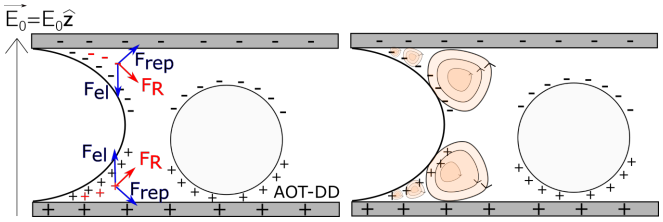


FIG. 8: Sketch of the electrohydrodynamic flow formation in the AOT/dodecane-$N_2$ interface. $F_{rep}$ represents the repulsive force the ion experiences due to the interface surface charge, $F_{el}$ the force due to the electric field and $F_R$ the resultant force.

Our experiments confirm that particles are attracted towards the interface and that they are kept at a separation $D$ away from it, which can be up to $\sim 400\mu m$ depending on the system.

We have studied how $D$ changes when changing $H$ and how it behaves when modifying $E_0$ for a constant $H$ (Fig. 9). From Fig. 9 we observe how the magnitude of these electrohydrodynamic flows, associated with the distance

$D$, indeed increases with $H$. However, modifying $E_0$ does not apparently change $D$.

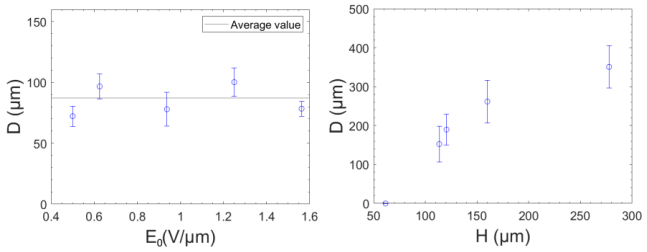


FIG. 9: Electrohydrodynamic flows dependence with the electric field and sample thickness. (a) Dependence between $D$ and $E_0$ for a system with $H = (160 \pm 3)\ \mu m$. (b) Dependence between $D$ and $H$.

### D. AOT/dodecane-Air interface

Finally, we have inquired about the effect of changing the AOT/dodecane-$N_2$ interface by an AOT/dodecane-air interface with $RH \sim 70\%$. In this case, we always observe the typical Quincke phenomenon along with a dramatic tendency of the particles to migrate and adsorb to the interface, where they form large steady aggregates. We believe that hydrodynamic long-range interactions are also present in these systems but that they are overwhelmed by possible image charge effects associated to the polarity of the air phase, which can lead to the binding of the particles to the interface [9].

## IV. CONCLUSIONS

We have shown how a system believed to interact mainly electrostatically has demonstrated to be more complex than it was initially supposed. Short-range effective attractions seen at $r < 3a$ have been attributed to dipole-dipole effects and long-range attractive interactions for $r > 3a$ have been attributed to electrohydrodynamic flows which have proved to play a key role in the system. These currents arise from ion motion due to the distortion of the electric field near the AOT/dodecane-particle and AOT/dodecane-air/$N_2$ interfaces. We have determined that the magnitude of this effect is thickness dependent and that it increases with it.

As a consequence of the long-range interactions, aligning and clustering have been observed and analysed. Particles locally align along the average direction of motion of their neighbours, showing alignment in systems with local packing fractions $\phi \geq 0.057 \pm 0.002$. In the clustering analyses, cluster stability has shown to not depend on $E_0$. However, increasing $E_0$ increases the number of clusters formed in the system. Smaller clusters are more stable than larger clusters.

The amount of experiments performed are but an initial amount and more experiments should be carried out to further confirm all our observations and interpretations. A further improvement to our experiment would be the design of a set-up that allows the variation of $H$ without having to manipulate the cell and the control of the amount of particles inserted. This set-up would allow a better study of the effect of thickness and density in the formation of the electrohydrodynamic currents.

### Acknowledgments

I want to specially thank Nikos Kyriakopoulos, Geet Raju and Jaakko Timonen for all their help, support and the opportunity to base my bachelor thesis on the data we collected in the laboratory of the Applied Physics department of Aalto university. I would also like to thank my advisor Alberto Fernández-Nieves for all the wonderful discussions we had and for making me enjoy physics even more.

[1] Y. Han and D. G. Grier, *Confinement-Induced Colloidal Attractions in Equilibrium*, Phys. Rev. Lett. **91**: 3 (2003).
[2] A. Bricard, J. B. Caussin, N. Desreumaux, O. Dauchot, and D. Bartolo, *Emergence of Macroscopic Directed Motion in Populations of Motile Colloids*, Nature **503**: 95 (2013).
[3] S. Q. Lu, B. Y. Zhang, Z. C. Zhang, Y. Shi and T. H. Zhang, *Pair aligning improved motility of Quincke rollers*, Soft Matter **14**: 5092 (2018).
[4] D. H. Kelley and N. T. Oullette, *Using particle tracking to measure flow instabilities in an undergraduate laboratory experiment*, American Journal of Physics **79**: 267 (2011).
[5] Q. Du, V. Faber and M. Gunzburger, *Centroidal Voronoi Tessellations: Applications and Algorithms*, SIAM Review **41**: 637 (1999).
[6] J. Sievers, VoronoiLimit(varargin), MATLAB Central File Exchange (2019).
[7] P. Jiang, J.F. Bertone, K.S. Hwang and V.L. Colvin, *Single-crystal colloidal multilayers of controlled thickness*, Chem. Mater. **11**: 2132 (1999).
[8] G. E. Pradillo, H. Karani and P. M. Vlahovska, *Quincke rotor dynamics in confinement: rolling and hovering*, Soft matter **15**: 6564 (2019).
[9] C. P. Kelleher et al., *Charged hydrophobic colloids at an oil–aqueous phase interface*, Physical Review E. **92**: 6 (2015).
[10] S. Yeh, M. Seul and B. Shraiman, *Assembly of ordered colloidal aggregates by electric-field-induced fluid flow*, Nature **386**: 57 (1997).